DALTON
FULL PAPER

Molecular structure of $Bu^tCl_2SiSiCl_2Bu^t$ in the gas phase by electron diffraction and *ab initio* calculations. Molecular structures of the compounds $Bu^tX_2SiSiX_2Bu^t$ (X = Cl, Br or I) by vibrational spectroscopy, X-ray crystallography and *ab initio* calculations †

Sarah L. Hinchley,[a] Bruce A. Smart,[a] Carole Morrison,[a] Heather E. Robertson,[a] David W. H. Rankin,*[a] Robert A. Coxall,[a] Simon Parsons,[a] Robert Zink,[b] Harald Siegl,[b] Karl Hassler *[b] and Richard Mawhorter[c]

[a] *Department of Chemistry, University of Edinburgh, West Mains Rd., Edinburgh, UK EH9 3JJ*
[b] *Institut für Anorganische Chemie, Technische Universität Graz, Stremayrgasse 16, A-8010 Graz, Austria*
[c] *Dept of Physics and Astronomy, Pomona College, 610 North College Avenue, Claremont, CA 91711-6359, USA*

Received 12th April 2001, Accepted 1st August 2001
First published as an Advance Article on the web 17th September 2001

The series of compounds $Bu^tX_2SiSiX_2Bu^t$ (X = Cl, Br and I) have been studied by X-ray crystallography, vibrational spectroscopy and *ab initio* calculations. The solids were all found to be *anti* and the vibrational spectra are consistent with this observation. The molecular structure of 1,2-di-*tert*-butyltetrachlorodisilane, $Bu^tCl_2SiSiCl_2Bu^t$, has also been determined in the gas phase by electron diffraction (GED) and *ab initio* molecular-orbital calculations. The conformation is distorted slightly from the fully staggered arrangement, with φ(CSiSiC) 167.7(11)°. Important structural parameters (r_a) include: Si–Si 238.0(7) pm, Si–C 187.2(7) pm, C–C 154.3(2) pm, C–H 114.2(4) pm, Si–Si–C 119.8(6)°, Cl–Si–Cl 105.5(8)° and C–Si–Si–C 167.7(11)°. These experimental observations are supported by theoretical predictions obtained at the MP2/6-31G* level.

Introduction

Structures and conformations of disilanes reflect both the steric and the electronic properties of the substituents. Electronic effects are demonstrated by shortening of the Si–Si bond distance as the hydrogen substituents in Si_2H_6[1] are replaced by electron-withdrawing F and Cl in Si_2F_6[2] and Si_2Cl_6,[3] or lengthened by the electron-releasing methyl groups in Si_2Me_6.[4] The structures of some disilanes partially substituted with larger bromine and iodine atoms, including 1,1,2,2-tetrabromodisilane,[5] 1,2-diiododisilane[6] and 1,1,2,2-tetraiododisilane,[6] have also been studied in the gas phase. In all of these examples, the favoured conformations are staggered about the Si–Si bonds.

However, systems containing the more sterically demanding *tert*-butyl groups are of greater structural interest, because the effect of the bulky alkyl ligands on the conformation of the groups around the silicon–silicon bond can lead to surprising results. In two compounds with just two *tert*-butyl groups, 1,2-di-*tert*-butyldisilane[7] and 1,2-di-*tert*-butyltetrafluorodisilane,[8] the transoid conformation was preferred, as expected, although for 1,2-di-*tert*-butyltetrafluorodisilane the data are consistent with a single conformer with a large-amplitude motion over a torsional range of around 140–220°.[8] In contrast, the most stable conformation of the even more sterically crowded 1,1,2-tri-*tert*-butyldisilane, the structure of which has recently been elucidated,[9] is the most unusual eclipsed arrangement, in which each butyl group eclipses a hydrogen atom at the opposite end of the molecule. This was found to be far more energetically favourable than either of the two possible staggered structures, which brought the butyl groups into closer contact.[9]

In view of the interesting and unusual conformational behaviour of the di- and tri-*tert*-butyl substituted disilanes, we have now undertaken further structural studies on the series of compounds $Bu^tX_2SiSiX_2Bu^t$, where X = Cl, Br and I. In these cases, the steric demands of the butyl groups must be accommodated in conjunction with the increasingly large halogen atoms. The gas-phase structure of 1,2-di-*tert*-butyltetrachlorodisilane has been determined, whilst the crystal structures have been obtained for all three molecules. Vibrational spectra have been recorded, and *ab initio* calculations have provided geometrical and vibrational information.

Experimental

Synthesis

The disilanes $Bu^tX_2SiSiX_2Bu^t$ were prepared according to the literature method.[10]

Ab initio calculations

All calculations at the HF level were performed on a Dec Alpha 1000 4/200 workstation using the Gaussian 94[11] and Gaussian 98[12] programs. An extensive search of the torsional potential of all the compounds was undertaken at the HF/3-21G*[13–15] level in order to locate all minima. For 1,2-di-*tert*-butyltetrachlorodisilane three non-equivalent conformers were found with φ(CSiSiC) 56, 94 and 169° (all C_2). For 1,2-di-*tert*-butyltetrabromodisilane and 1,2-di-*tert*-butyltetraiododisilane, two non-equivalent conformers were found with 56 and 168°

† Electronic supplementary information (ESI) available: tables of geometrical parameters and calculated and observed wavenumbers for $Bu^tX_2SiSiX_2Bu^t$ (X = Cl, Br, I). See http://www.rsc.org/suppdata/dt/b1/b103315h/

 DOI: 10.1039/b103315h

(both C_2) for the bromo analogue and 55 and 170° (both C_2) for the iodo analogue. Further geometry optimisations were undertaken at the HF and MP2 (frozen-core) levels using the standard 6-31G* [16–18] basis set for the chloro analogue. For the bromo and iodo analogues, the Stevens–Basch–Krauss effective core potential [19–21] with polarisation functions (CEP-41G*) were used on the bromine and iodine atoms, with the 6-31G* basis set used on the silicon, carbon and hydrogen. It should be noted that there is only one CEP basis set defined for atoms beyond the second row. HF and MP2 calculations for 1,2-di-*tert*-butyltetrabromodisilane and 1,2-di-*tert*-butyltetraiododisilane were carried out using resources of the UK Computational Chemistry Facility, on a DEC 8400 superscalar cluster equipped with 10 fast processors, 6 GB of memory and a 150 GB disk.

Vibrational frequencies, calculated from analytic second derivatives at the HF/3-21G* and HF/6-31G* levels were used to determine the nature of stationary points for all the molecules. They also provided estimates of amplitudes of vibration (u) for use in the gas electron diffraction (GED) refinement and comparison with experimentally determined frequencies for 1,2-di-*tert*-butyltetrachlorodisilane.

The nomenclature we will use for the conformers located is that proposed by Josef Michl,[22] in which a convention for the labelling of conformations as *anti*, transoid, deviant, *ortho*, *gauche*, cisoid and *syn* depending on the dihedral angle is outlined.

X-Ray crystallography

Crystal data for 1,2-di-*tert*-butyltetrachlorodisilane (see Table 1). Data were collected on an APEX SMART CCD diffractometer. 2182 reflections were collected (1420 unique, R_{int} = 0.0245). The structure was solved by direct methods and refined against F^2 (SHELXTL),[23] yielding R_1 = 0.0380, for 1155 independent reflections with $F > 4\delta(F)$, $wR_2 = 0.0933$. All non-H atoms were refined with anisotropic thermal parameters, with H-atoms placed in calculated positions.

Crystal data for 1,2-di-*tert*-butyltetrabromodisilane (see Table 1). Data were collected on a Stöe diffractometer. 2709 reflections were collected (2303 unique, $R_{int} = 0.0459$). The structure was solved by direct methods and refined against F^2 (SHELXTL),[23] yielding $R_1 = 0.0704$, with $wR_2 = 0.1902$. All non-H atoms were refined with anisotropic thermal parameters, with H-atoms placed in calculated positions.

Crystal data for 1,2-di-*tert*-butyltetraiododisilane (see Table 1). Data were collected on a Stöe diffractometer. 4467 reflections were collected (3869 unique, $R_{int} = 0.0241$). The structure was solved by direct methods and refined against F^2 (SHELXTL),[23] yielding $R_1 = 0.0618$ with $wR_2 = 0.1733$. All non-H atoms were refined with anisotropic thermal parameters, with H-atoms placed in calculated positions.

Structure solution and refinement

See Table 1(c). Weighting schemes adopted for the three systems were $w^{-1} = [\sigma^2(F_o^2) + (0.0490P)^2 + 0.0000P]$ where $P = [1/3 (F_o^2 + 2F_c^2)]$ for 1,2-di-*tert*-butyltetrachlorodisilane, $w^{-1} = [\sigma^2(F_o^2) + (0.1095P)^2 + 1.99P]$ where $P = [1/3 (F_o^2 + 2F_c^2)]$ for 1,2-di-*tert*-butyltetrabromodisilane $w^{-1} = [\sigma^2(F_o^2) + (0.1095P)^2 + 1.99P]$ where $P = [1/3 (F_o^2 + 2F_c^2)]$ for 1,2-di-*tert*-butyltetraiododisilane.

CCDC reference numbers 169479–169481.

See http://www.rsc.org/suppdata/dt/b1/b103315h/ for crystallographic data in CIF or other electronic format.

Infrared and Raman spectra

Infrared spectra (range from 3000–250 cm^{-1}) and variable temperature Raman spectra were measured as described previously.[9]

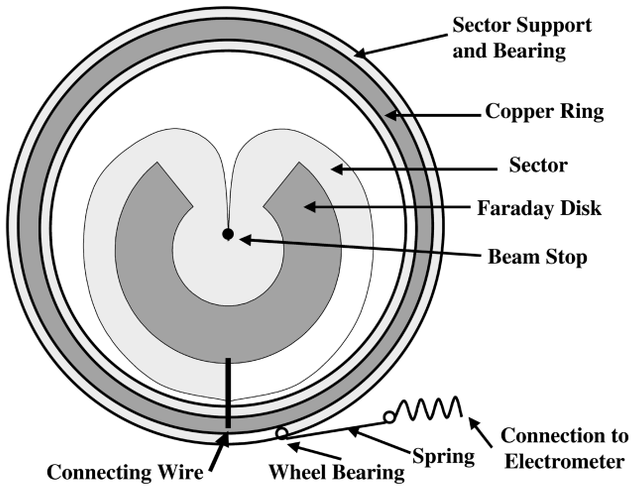

Fig. 1 Arrangement of the Faraday disk mounted on the rotating sector of the Edinburgh electron diffraction apparatus.

Electron diffraction

Electron scattering intensities were recorded on Kodak Electron Image plates using the Edinburgh gas diffraction apparatus operating at *ca*. 44.5 kV (electron wavelength *ca.* 5.6 pm).[24] Nozzle-to-plate distances for the metal inlet nozzle were *ca.* 94 and 259 mm yielding data in the s range 20–356 nm^{-1}. The sample and nozzle temperatures were maintained at *ca.* 455 K during the exposure periods.

The scattering patterns of benzene were also recorded for the purpose of calibration; these were analysed in exactly the same way as those for $Bu^tCl_2SiSiCl_2Bu^t$ so as to minimise systematic errors in the wavelengths and camera distances. Nozzle-to-plate distances, weighting functions used to set up the off-diagonal weight matrix, correlation parameters, final scale factors and electron wavelengths for the measurements are collected in Table 2.

The electron-scattering patterns were converted into digital form using a PDS densitometer at the Institute of Astronomy in Cambridge with a scanning program described elsewhere.[25] The programs used for data reduction [26] and least-squares refinement [27] have been described previously; the complex scattering factors were those listed by Ross *et al*.[28]

Exposure times needed to give the ideal optical density on the plates can be estimated accurately using a Faraday disk mounted on the rotating sector. The arrangement is shown in Fig. 1.

The disk (part of an annulus) is mounted on insulators on the sector, and is connected by a fixed wire to a copper ring, also mounted on insulators, on the sector support ring. A small wheel, linked to a spring, bears on the outside surface of the copper ring. The other end of the spring is attached to the fixed part of the sector assembly (again insulated), and a wire then provides a link to an electrometer. A fixed fraction of the total scattering can thus be monitored, both before and during the exposures. Poor exposure of plates has effectively been eliminated using this arrangement.

Results

Ab initio calculations

Extensive searches of the torsional potential of all three molecules led to the location of three minima for 1,2-di-*tert*-butyltetrachlorodisilane, two for 1,2-di-*tert*-butyltetrabromodisilane, and two for 1,2-di-*tert*-butyltetraiododisilane. Vibrational frequency calculations at the HF/6-31G* level for

Table 1 X-Ray crystal structures, (a) crystal data, (b) data collection and processing, (c) structure solution and refinement

	$Bu^tCl_2SiSiCl_2Bu^t$	$Bu^tBr_2SiSiBr_2Bu^t$	$Bu^tI_2SiSiI_2Bu^t$
(a) Crystal data			
Empirical formula	$C_8H_{18}Cl_4Si_2$	$C_8H_{18}Br_4Si_2$	$C_8H_{18}I_4Si_2$
M	312.2	490.04	678.00
Wavelength	0.71073 Å	0.71073 Å	0.71073 Å
Temperature	150(2) K	293(2) K	293(2) K
Crystal system	Triclinic	Triclinic	Triclinic
Space group	$P\bar{1}$	$P\bar{1}$	$P\bar{1}$
Unit cell dimensions	a = 6.7183(17) Å, α = 94.93(4)°	a = 7.0720(10) Å, α = 96.49(3)°	a = 7.639(2) Å, α = 100.11(3)°
	b = 7.5290(19) Å, β = 107.60(3)°	b = 7.637(2) Å, β = 108.36(3)°	b = 8.033(2) Å, β = 106.83(3)°
	c = 8.789(2) Å, γ = 112.43(4)°	c = 8.827(2) Å, γ = 114.02(3)°	c = 8.854(2), Å, γ =114.77(3)°
Volume	381.35(16) Å^3	397.0(2) Å^3	443.8(2) Å^3
Number of reflections for cell	1828 ($5 < \theta < 52°$)	—	—
Z	1	1	1
Density (calculated)	1.359 Mg m^{-3}	2.050 Mg m^{-3}	2.537 Mg m^{-3}
Absorption coefficient	0.901 mm^{-1}	10.259 mm^{-1}	7.130 mm^{-1}
F(000)	162	234	306
(b) Data collection			
Crystal description	Colourless cylinder	Colourless needles	Colourless needles
Crystal size	0.40 × 0.17 × 0.17 mm	*ca.* 0.30 × 0.15 × 0.15 mm	*ca.* 0.30 × 0.15 × 0.15 mm
θ range	2.50 to 26.36°	3.04 to 30.00°	2.97 to 34.97°
Index ranges	$-7 \le h \le 8$, $-9 \le k \le 8$,	$-9 \le h \le 9$, $-10 \le k \le 10$,	$-12 \le h \le 11$, $-12 \le k \le 12$,
	$-10 \le l \le 10$	$-12 \le l \le 12$	$-12 \le l \le 14$
Reflections collected	2182	2709	4467
Independent reflections	1420 (R_{int} = 0. 0245)	2303 (R_{int} = 0. 0459)	3869 (R_{int} = 0. 0241)
Scan type	φ and ω scans	—	—
Absorption correction	Empirical (T_{min} = 0.533,	—	—
	T_{max} = 0.962)		
(c) Solution and refinement			
Solution	Direct (SHELXS-97)	Direct (SHELXS-93)	Direct (SHELXS-93)
Refinement type	Full-matrix least-squares on F^2	Full-matrix least-squares on F^2	Full-matrix least-squares on F^2
Program used for refinement	SHELXTL	SHELXTL	SHELXTL
Hydrogen atom placement	Geometric	Geometric	Geometric
Hydrogen atom treatment	Riding, rotation groups Me	Riding, rotation groups Me	Riding, rotation groups Me
Data/restraints/parameters	1420/0/67	2301/0/67	3868/0/67
Goodness-of-fit on F^2	0.944	1.303	1.180
Conventional R [$F \ge 4\sigma(F)$]	R_1 = 0.0380 (1155 data)	R_1 = 0.0704 [$I > 2\sigma(I)$]	R_1 = 0.0618 [$I > 2\sigma(I)$]
Weighted R (F^2 and all data)	wR_2 = 0.0933	wR_2 = 0.1902	wR_2 = 0.1733
Final maximum δ/σ	0	—	—
Largest diff. peak and hole	0.688 and −0.321 e Å^{-3}	2.540 and −2.597 e Å^{-3}	4.777 and −6.520 e Å^{-3}

Table 2 Nozzle-to-plate distances (mm), weighting functions (nm^{-1}), correlation parameters, scale factors and electron wavelengths (pm) used in the electron diffraction study

Nozzle-to-plate distance[a]	Δs	s_{min}	sw_1	sw_2	s_{max}	Correlation parameter	Scale factor[b]	Electron wavelength
93.34	4	100	120	270	300	−0.0777	0.556(23)	5.655
258.02	2	20	40	144	168	0.1907	0.831(21)	5.654

[a] Determined by reference to the scattering pattern of benzene vapour. [b] Values in parentheses are the estimated standard deviations.

1,2-di-*tert*-butyltetrachlorodisilane and the HF/CEP-4G* level for the bromo and iodo analogues confirm that all the forms represent local minima on the potential energy surface. The three tetrachloro conformers with φ(CSiSiC) 163.8, 94.6 and 56.4° had relative energies of 0, 8.84 and 8.35 kJ mol^{-1}. This equates to a mixture containing 93.8% of the transoid conformer, and 3.4 and 2.8% of the 94 and 56° conformers, respectively, at room temperature. The two tetrabromo conformers with φ(CSiSiC) 165.8 and 55.2° had relative energies of 0 and 5.6 kJ mol^{-1}. This would equate to a mixture containing 89.6% of the transoid conformer, and 10.4% of the *gauche* conformer at room temperature. The two tetraiodo conformers with φ(CSiSiC) 168.1 and 53.0° had relative energies of 0 and 1.6 kJ mol^{-1}. This would equate to a mixture containing 52.4% of the transoid conformer, and 47.6% of the *gauche* conformer at room temperature.

As the transoid conformer is dominant in each case, discussion will focus on these structures. The molecular geometries of these conformers at the MP2/6-31G* level for 1,2-di-*tert*-butyltetrachlorodisilane and the MP2/CEP-4G* level for the bromo and iodo analogues are presented in Table 3; those calculated at lower levels of theory are presented in Table S1 (ESI). The molecular geometries of the highest level calculations for the other conformations of 1,2-di-*tert*-butyltetrachlorodisilane, 1,2-di-*tert*-butyltetrabromodisilane and 1,2-di-*tert*-butyltetraiododisilane are presented in Table S2 (ESI).

As expected, since these systems contain no multiple bonds or lone pairs of electrons, the molecular geometry of the conformers proved to be relatively insensitive to changes in the theoretical method. For this reason, only the highest level results (MP2/6-31G*) will be discussed and presented in the order 1,2-di-*tert*-butyltetrachlorodisilane, 1,2-di-*tert*-butyltetrabromodisilane and 1,2-di-*tert*-butyltetraiododisilane where multiple results are discussed.

The molecular geometries appear to be dictated predominately by steric and, to a lesser extent, electronic interactions, as

Table 3 Theoretical geometrical parameters for the transoid conformers of 1,2-di-*tert*-butyltetrachlorodisilane (C_2, MP2/6-31G*), 1,2-di-*tert*-butyltetrabromodisilane (C_2, MP2/CEP-4G*)[a] and 1,2-di-*tert*-butyltetraiododisilane (C_2, MP2/CEP-4G*)[a,b]

	$Bu^tCl_2SiSiCl_2Bu^t$	$Bu^tBr_2SiSiBr_2Bu^t$	$Bu^tI_2SiSiI_2Bu^t$
Si(1)–Si(2)	235.7	238.4	238.0
Si(2)–C(21)	188.9	190.0	191.3
C(21)–C(211)	153.5	155.0	153.5
C(21)–C(212)	153.6	154.9	153.5
C(21)–C(213)	153.6	155.0	153.6
Si(2)–X(22)	207.1	225.2	248.4
Si(2)–X(23)	207.3	225.4	248.5
C–H[c]	109.5	111.4	109.5
Si(1)–Si(2)–C(21)	117.6	117.7	117.1
Si(2)–C(21)–C(211)	109.1	108.7	109.2
Si(2)–C(21)–C(212)	110.0	109.6	109.7
Si(2)–C(21)–C(213)	108.9	110.1	110.6
Si(1)–Si(2)–X(22)	105.4	104.8	106.3
Si(1)–Si(2)–X(23)	108.2	108.9	109.3
C–C–H[c]	110.9	110.9	110.9
C(21)–Si(2)–Si(1)–C(11)	167.8	165.8	168.1
Absolute energy/Hartrees	−2721.1717	−116.2439	−937.6514

[a] 6-31G* on C, Si, H and CEP-4G* on Br and I. See text for details. [b] All distances in pm, all angles in degrees. See Fig. 2 for atom numbering. [c] Average value.

evident in the predicted values of the Si(1)–Si(2)–C(21) angle. This angle was predicted to be 117.6, 117.7 and 117.1° compared to 109.5° for an ideal tetrahedral geometry around the silicon atom. In contrast, the X(22)–Si(2)–X(23) angles were predicted to be 107.4, 107.0 and 107.5°, possibly indicating that the bulk of the *tert*-butyl groups is forcing the halogen atoms closer together. This could also be attributed to an electronic effect of the electron-withdrawing halogen atoms. The Si–Si–C angles are similar to those calculated for 1,2-di-*tert*-butyltetrafluorodisilane[8] (117.6°) and 1,2-di-*tert*-butyldisilane[7] (114.4°). The internal C–C–C angles (109.6, 109.4 and 109.1°) indicate that the *tert*-butyl groups are hardly distorted from local C_3 symmetry in all the molecules studied.

Bond length predictions are generally within the expected ranges based on the results obtained previously for disilanes with *tert*-butyl or halogen groups. For example, the Si–Si bond lengths were predicted to be 235.7, 238.4 and 238.0 pm respectively, compared to 234.9 pm in 1,2-di-*tert*-butyltetrafluorodisilane[8] and 236.8 pm in 1,2-di-*tert*-butyldisilane.[7] All the predicted C–C bond lengths were similar (153.5, 155.0 and 153.5 pm), as were the Si–C bond lengths (188.9, 190.0 and 191.3 pm). This falls within a range of Si–C bonds previously observed, for example 1.882(1) and 1.886(1) pm for 1,4-disilabutane and 1,5-disilapentane,[30] and 191.9 pm in 1,2-di-*tert*-butyldisilane[7]. The Si–Cl bond lengths were predicted to be 207.1 and 207.3 pm, which compare well to that found experimentally in 1,2-dichlorotetramethyldisilane[31] [207.7(2) pm] but are significantly longer than in 1,1,2,2-tetrachlorodisilane[32] [203.9(2) pm (average value)]. The Si–Br bond lengths were predicted to be 225.2 and 225.4 pm which are both longer than found experimentally in 1,1,2,2-tetrabromodisilane[5] [220.5(5) pm]. The Si–I bond lengths were predicted to be 248.4 and 248.5 pm which again are much longer than those found experimentally in 1,2-diiododisilane[6] [242.9(13) pm] and 1,1,2,2-tetraiododisilane[6] [244.0(9) pm].

Gas electron diffraction model for 1,2-di-*tert*-butyltetrachlorodisilane

On the basis of the *ab initio* calculations described above, electron diffraction refinements were carried out using a model of the transoid conformation (C_2 symmetry) of 1,2-di-*tert*-butyltetrachlorodisilane to describe the vapour. The large number of geometric parameters needed to define the model made it necessary to make a number of assumptions, including local C_{3v} symmetry for all methyl groups and local C_3 symmetry for the *tert*-butyl groups. These assumptions are justified by the *ab initio* results. Initially, some of the differences between similar bond lengths and bond angles were restrained using the SARACEN[29] method. However, since many of these difference parameters proved to be uncorrelated with other refining parameters, and returned values and e.s.d.'s which were close to the restraints, they were fixed in the final refinement. We can therefore be confident that the refined parameters, and their e.s.d.'s, are not affected significantly by the assumptions applied to the molecular model.

The structure of $Bu^tCl_2SiSiCl_2Bu^t$ was finally defined in terms of seventeen independent geometric parameters, comprising five bond lengths, five bond angles and seven torsion and tilt parameters, and four dependent parameters comprising four bond angles [Table 4; atom numbering shown in Fig. 2(a)].

The independent parameters include the C–H and C–C bond lengths (p_1 and p_2), and average bond lengths for the Si–Si, Si–C and Si–Cl bonds (p_3–p_5), with small differences between non-equivalent bond lengths fixed at the *ab initio* values. All C–C–H bond angles (p_6) were assumed to be identical, as were all C–C–C bond angles (p_7). The Si–Si–C angle was also included (p_8). The Si–Si–Cl angles were defined in terms of the average (p_9) of Si(2)–Si(1)–Cl(12) and Si(2)–Si(1)–Cl(13) and the difference (p_{10}) between the two angles.

Of the remaining seven parameters, two represent the torsion and tilt of the *tert*-butyl groups. These groups were generated initially by placing a methyl group carbon atom at the origin, with its three H atoms arranged with local C_{3v} symmetry about the x axis and one H in the xy plane in the positive x and y directions. The methyl torsion and tilt parameters (p_{11}, p_{12}) are rotations about the local x and y axes respectively. The methyl group is then translated along the positive x axis by the C–C bond length and the central carbon of the *tert*-butyl group is placed at the origin. The correct C–C–C bond angles are generated by rotating the methyl group about the z axis, moving the methyl carbon atom in the positive y direction, and then generating the other methyl groups by rotation of the first group about the x axis by 120 or −120°, respectively. The *tert*-butyl torsion angle is a rotation of the group about the x axis (p_{13}).

The tilt parameter is a rotation of the whole butyl group about the y axis (p_{14}). A positive tilt would move the butyl group with C(21) at the centre away from that with C(11) at the centre in the local y direction of the butyl groups.

Having generated the *tert*-butyl groups in their local coordinate systems, they need to be rotated about the x axis to put them in the correct position relative to the silicon atoms. The *tert*-butyl group and the two chlorines attached to Si(1) were

Table 4 Refined and calculated geometric parameters for 1,2-di-*tert*-butyltetrachlorodisilane (distances in pm, angles in degrees) from the GED study[a]

No.	Parameter	GED (r_a)	MP2/6-31G* (r_e)
Independent parameters			
p_1	C–H (mean)	114.2(4)	109.5
p_2	C–C (mean)	154.3(2)	153.6
p_3	Si–Si	238.0(7)	235.8
p_4	Si–C	187.2(7)	188.9
p_5	Si–Cl (mean)	207.1(1)	207.2
p_6	C–C–H	109.2(9)	110.9
p_7	C–C–C	109.1(3)	109.4
p_8	Si–Si–C	119.8(6)	117.6
p_9	Si–Si–Cl (mean)	105.2(3)	106.8
p_{10}	Si–Si–Cl (diff)	1.8(5)	2.8
p_{11}	Me twist	176.6(21)	178.3
p_{12}	Me tilt	2.5(19)	—
p_{13}	Bu^t twist	167.5(17)	171.1
p_{14}	Bu^t tilt	2.3(8)	—
p_{15}	Cl torsion (mean)[b]	124.4(5)	122.7
p_{16}	Cl torsion (diff)[c]	2.8(11)	2.1
p_{17}	CSiSiC	167.7(11)	167.9
Dependent parameters			
p_{18}	Si–C–C(211)	109.3(4)	109.1
p_{19}	Si–C–C(212)	112.0(8)	110.0
p_{20}	Si–C–C(213)	108.2(7)	108.9
p_{21}	Cl–Si–Cl	105.5(8)	106.1

[a] Figures in parentheses are the estimated standard deviations of the last digits. See text for parameter definitions. [b] Average of torsions C(11)–Si(1)–Si(2)–Cl(12) and C(11)–Si(1)–Si(2)–Cl(13). [c] Difference C(21)–Si(2)–Si(1)–Cl(12) minus C(21)–Si(2)–Si(1)–Cl(13).

initially placed in the *xy* plane, and the chlorine atoms were then rotated about the *x* axis. These rotations are defined in terms of the average of the torsion angles C(11)–Si(1)–Si(2)–Cl(12) and C(11)–Si(1)–Si(2)–Cl(13) (p_{15}) and the difference between these two angles. Finally, the dihedral angle C(21)–Si(2)–Si(1)–C(11) (p_{17}) described the overall conformation about the Si–Si bond, with a value of zero indicating the conformation in which the two central carbon atoms of the *tert*-butyl groups were eclipsing one another.

Four dependent parameters were also used, describing the SiCC angles to the methyl carbon atoms and the ClSiCl angle.

Gas-phase electron diffraction (GED) refinement of 1,2-di-*tert*-butyltetrachlorodisilane

The starting parameters for the r_a refinement were taken from the theoretical geometry optimised at the MP2/6-31G* level. The r_a structure was not determined because the rectilinear vibrational corrections (*i.e.* parallel and perpendicular correction terms) are known to be unreliable for a molecule of this size, with many low-lying vibrational modes. Theoretical (HF/6-31G*) Cartesian force fields were obtained and converted into force fields described by a set of symmetry coordinates using the ASYM40 program.[33] All geometric parameters were then refined.

In total seventeen geometric parameters and thirty groups of vibrational amplitudes were refined. Eight geometric and twenty-four amplitude flexible restraints were employed using the SARACEN method.[29] These are listed in Tables S3 and S4 (ESI).

The success of the final refinement, for which $R_G = 0.075$ ($R_D = 0.065$), can be assessed on the basis of the molecular scattering intensity curves (Fig. 3) and the radial distribution curve (Fig. 4). Final refined parameters are listed in Table 4, interatomic distances and the corresponding amplitudes of vibration in Table 5, with the least-squares correlation matrix shown in Table S5 and the experimental coordinates from the GED analysis in Table S6 (ESI). In the SARACEN[29] analysis, all correlation between refining parameters is allowed for in the error estimates by the use of flexible restraints. We therefore quote the estimated standard deviations, σ, and believe that these are realistic estimates of the uncertainties of the parameters.

Fig. 2(a) shows a perspective view of the transoid conformer of $Bu^tCl_2SiSiCl_2Bu^t$ in the optimum refinement of the GED data.

Crystal structure determination

All three solid structures were found to possess $P\bar{1}$ symmetry. Most of the common parameters associated with the structures agree to within 1–2 pm or 1–2°. For example, the Si–Si bond lengths were found to be 236.9, 235.5 and 236.6 pm for the chloro, bromo and iodo analogues respectively, whilst the mean C–C distances were 154.3, 153.7 and 154.0 pm. A gradual lengthening of the Si–C bond was observed from the chloro to iodo compound (188.1, 189.7 and 190.4 pm). Si–Cl bond lengths were observed to be 206.6 and 206.1 pm, whilst Si–Br bond lengths were 221.8 and 223.2 pm and Si–I bond lengths were 246.1 and 246.8 pm. The mean CCC angles within the butyl groups were found to agree extremely well, 109.5° in 1,2-di-*tert*-butyltetrachlorodisilane, 110.1° in 1,2-di-*tert*-butyltetrabromodisilane and 109.2° in 1,2-di-*tert*-butyltetraiododisilane. The SiSiC angles were found to increase slightly from chlorine to bromine to iodine (118.2 to 119.2 to 120.0°). SiSiX angles were found to be 107.2 and 106.4° for 1,2-di-*tert*-butyltetrachlorodisilane, 106.1 and 106.5° for 1,2-di-*tert*-butyltetrabromodisilane and 106.7 and 105.4° for 1,2-di-*tert*-butyltetraiododisilane, whilst the XSiX angles were 106.9, 107.6 and 108.1° respectively. Geometrical parameters obtained for all three compounds by X-ray crystallography are presented in Table S7 (ESI).

Vibrational spectra and normal coordinate analyses

The molecules $Bu^tX_2SiSiX_2Bu^t$ (where X = Cl, Br or I) have 90 fundamental modes which distribute in the following way between the symmetry species of the hypothetical perfectly staggered *anti* structure (point group C_{2h}) and the *gauche* structure (point group C_2): *anti* (C_{2h}): $\Gamma_{vib} = 25\ a_g$ (Raman) + $20\ b_g$ (Raman) + $21\ a_u$ (IR) + $24\ b_u$ (IR), *gauche* (C_2): $\Gamma_{vib} = 46$ a (IR, Raman) + 44 b (IR, Raman).

Table 5 Selected interatomic distances and mean amplitudes of vibration for 1,2-di-*tert*-butyltetrachlorodisilane from the GED study[a]

No.	Atom pair	r_a/pm	u/pm
1	Si(1)–Si(2)	238.0(7)	6.5(6)
2	Si(2)–C(21)	187.2(7)	7.1(7)
3	Si(2)–Cl(22)	206.9(1)	5.6(3)
4	C–C	154.3(2)	6.9(4)
5	C–H	114.2(4)	8.7(5)
6	Cl(22)···Cl(23)	329.8(17)	12.5(9)
7	C(211)···C(212)	251.4(6)	7.1(7)
8	Si(1)···C(21)	368.8(14)	10.8(10)
9	Si(1)···C(211)	499.5(11)	9.7(20)
10	Si(1)···C(212)	420.7(28)	22.7(21)
11	Si(2)···C(211)	279.2(4)	9.1(5)
12	C(11)···C(21)	533.1(21)	14.2 (fixed)
13	Si(1)···Cl(22)	349.6(13)	13.0(12)
14	Si(1)···Cl(23)	358.3(15)	12.5(10)
15	C(21)···Cl(22)	323.5(32)	10.6(10)
16	C(21)···Cl(23)	323.1(34)	10.5 (tied to u_{15})

[a] See Fig. 2 for atom numbering. (Other amplitudes were used in the refinement but are not shown here.) A full list of the heavy atom distances and amplitudes of vibration is given in Table S11 (ESI).

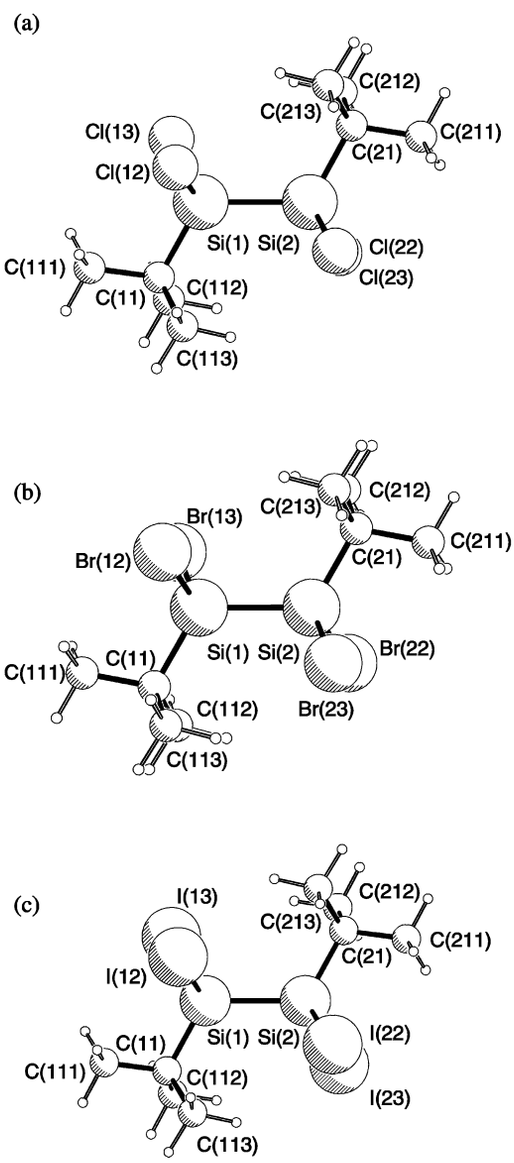

Fig. 2 Molecular structures of (a) 1,2-di-*tert*-butyltetrachlorodisilane, (b) 1,2-di-*tert*-butyltetrabromodisilane and (c) 1,2-di-*tert*-butyltetraiododisilane.

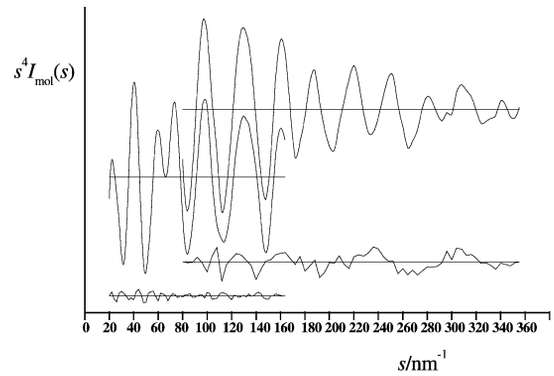

Fig. 3 Experimental and difference (experimental − theoretical) radial distribution curves, $P(r)/r$, for $Bu^tCl_2SiSiCl_2Bu^t$. Before Fourier inversion the data were multiplied by $s\cdot\exp(-0.00002s^2)/(Z_{Si} - f_{Si})/(Z_{Cl} - f_{Cl})$, where $s = (4\pi \sin \theta)/\lambda$, f is the scattering factor and Z is the atomic number.

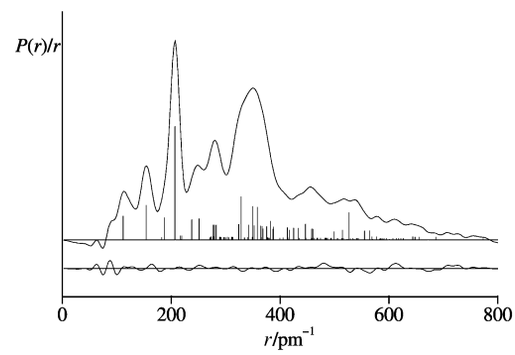

Fig. 4 Experimental and final weighted difference (experimental − theoretical) molecular-scattering intensities for 1,2-di-*tert*-butyltetrachlorodisilane.

The spectral positions of methyl stretching and deformation modes ($\nu_{sym}CH_3$, $\nu_{asym}CH_3$, $\delta_{sym}CH_3$ and $\delta_{asym}CH_3$) are of little interest. Exclusion of these modes from further discussion simplifies the vibrational problem to:

anti (C_{2h}): Γ_{vib} = 15 a_g (Raman) + 12 b_g (Raman) + 13 a_u (IR) + 14 b_u (IR), *gauche* (C_2): Γ_{vib} = 28 a (IR, Raman) + 26 b (IR, Raman).

To characterise the calculated vibrational modes, normal coordinate and potential energy distribution (PED) analyses have been carried out following the Wilson FG method[34] utilizing the calculated optimised structures and Cartesian force constants. The Cartesian Hessian matrices were thereby transformed into force fields defined in symmetry coordinates, which were linear combinations of redundant internal coordinates, resulting in a description of normal modes in terms of symmetry coordinates according to the PED values. The ASYM40[33] program was used for these computations. The chosen symmetry coordinates are listed in Table 6. The measured vibrational wavenumbers are collected in Table 7. Tables S8–10 (ESI) summarise experimental wavenumbers, scaled theoretical wavenumbers and the tentative description of the modes by a single symmetry coordinate according to the PED values. For reasons of clarity and available space only calculated PED values for the transoid conformers have been listed. Moreover, the following discussion also focuses on the transoid species and uses the symmetry species of the hypothetical perfectly staggered structures.

Inspection of the computed PED values shows that the description of normal modes by a single symmetry coordinate is highly approximate since several modes represent mixtures of

Table 6 Symmetry coordinates for $Bu^tX_2SiSiX_2Bu^t$ [a]

Species [b]	No.	Description	Species [b]	No.	Description
a_g	S_1	ρ_1CH_3 (CH_3 rock)	b_g	S_{29}	ρ_1CH_3 (CH_3 rock)
	S_2	ρ_2CH_3 (CH_3 rock)		S_{30}	ρ_2CH_3 (CH_3 rock)
	S_3	ρ_3CH_3 (CH_3 rock)		S_{31}	ρ_3CH_3 (CH_3 rock)
	S_4	$\nu_{sym}CC_3$ (CC_3 sym stretch)		S_{32}	$\nu_{asym}CC_3$ (CC_3 asym stretch)
	S_5	$\nu_{asym}CC_3$ (CC_3 asym stretch)		S_{33}	$\delta_{asym}CC_3$ (CC_3 asym def)
	S_6	$\delta_{sym}CC_3$ (CC_3 sym def)		S_{34}	ρCC_3 (CC_3 rock)
	S_7	$\delta_{asym}CC_3$ (CC_3 asym def)		S_{35}	$\nu_{asym}SiX_2$ (SiX_2 asym stretch)
	S_8	ρCC_3 (CC_3 rock)		S_{36}	τSiX_2 (SiX_2 twist)
	S_9	νSiC (SiC stretch)		S_{37}	ρSiX_2 (SiX_2 rock)
	S_{10}	$\nu_{sym}SiX_2$ (SiX_2 sym stretch)		S_{38}	τ_1CC (CC torsion)
	S_{11}	νSiSi		S_{39}	τ_2CC (CC torsion)
	S_{12}	δSiSiC (SiSiC def)		S_{40}	τSiC (SiC torsion)
	S_{13}	δSiX_2 (SiX_2 scissoring)	b_u	S_{41}	ρ_1CH_3 (CH_3 rock)
	S_{14}	γSiX_2 (SiX_2 wag)		S_{42}	ρ_2CH_3 (CH_3 rock)
	S_{15}	τCC (CC torsion)		S_{43}	ρ_3CH_3 (CH_3 rock)
a_u	S_{16}	ρ_1CH_3 (CH_3 rock)		S_{44}	$\nu_{sym}CC_3$ (CC_3 sym stretch)
	S_{17}	ρ_2CH_3 (CH_3 rock)		S_{45}	$\nu_{asym}CC_3$ (CC_3 asym stretch)
	S_{18}	ρ_3CH_3 (CH_3 rock)		S_{46}	$\delta_{sym}CC_3$ (CC_3 sym def)
	S_{19}	$\nu_{asym}CC_3$ (CC_3 asym stretch)		S_{47}	$\delta_{asym}CC_3$ (CC_3 asym def)
	S_{20}	$\delta_{asym}CC_3$ (CC_3 asym def)		S_{48}	ρCC_3 (CC_3 rock)
	S_{21}	ρCC_3 (CC_3 rock)		S_{49}	νSiC (SiC stretch)
	S_{22}	$\nu_{asym}SiX_2$ (SiX_2 asym stretch)		S_{50}	$\nu_{sym}SiX_2$ (SiX_2 sym stretch)
	S_{23}	τSiX_2 (SiX_2 twist)		S_{51}	δSiSiC (SiSiC def)
	S_{24}	ρSiX_2 (SiX_2 rock)		S_{52}	δSiX_2 (SiX_2 scissoring)
	S_{25}	τ_1CC (CC torsion)		S_{53}	γSiX_2 (SiX_2 wag)
	S_{26}	τ_2CC (CC torsion)		S_{54}	τCC (CC torsion)
	S_{27}	τSiC (SiC torsion)			
	S_{28}	τSiSi (SiSi torsion)			

[a] Symmetry coordinates for methyl stretching and deformation modes have been omitted. [b] Symmetry species corresponding to the hypothetical planar (*anti*) structure of C_{2h} symmetry. The a_g and a_u blocks and the b_g and b_u blocks combine to a and b blocks, respectively, for the point group C_2 of transoid and twisted (*gauche*, *ortho*) conformers.

Table 7 Infrared and Raman spectra (<1250 cm^{-1}) of solid $Bu^tX_2SiSiX_2Bu^t$ (X = Cl, Br and I) [a]

$Bu^tCl_2SiSiCl_2Bu^t$		$Bu^tBr_2SiSiBr_2Bu^t$		$Bu^tI_2SiSiI_2Bu^t$	
IR	Raman	IR	Raman	IR	Raman
1204m	1227w,sh				
	1202s		1200sh		1182m
1185m	1188sh	1193ms	1186ms	1169m	1167sh
1006s	1006w	1004ms	1007m	1005m	1005w
940s	939w	939m	939m	937m	938w
815vs	814s	809s	810s	804ms	806m
					800sh
670vvw		620sh	622m		601mw
630sh	632s	601s			
616vs					
587m,sh	585w	561mw		584m	
562vvs	548w	534vw	537w	543w	
525vw		516mw		489w	502mw
483vs		474vs	470m	424vs	425m
443m	437vs	425sh	421sh	390sh	396m
396vs	391vw	407vs	410s	374vs	375m
352vs	383w	390sh	381m	355sh	
	307ms	342s		327vs	
279m	289w		284sh		276vw,b
	274w				239sh
	264w		244m		230w,b
	233ms		223vs		198vs
	186s		158w		
	158w		141vs		
	137vs		131s		
	130s		114s		118s
	110ms		96s		100vs
	49w		77vs		80s
	34w				55vs
					30w

[a] s = Strong, m = medium, w = weak, v = very, sh = shoulder, b = broad. All values in cm^{-1}.

two, three or even more dominant symmetry coordinates, and sometimes a symmetry coordinate is the most important contribution in two different modes (see Tables S8–10, ESI).

The vibrational spectra can be divided into regions dominated by methyl rocking vibrations, CC, SiC, SiSi and SiX stretching modes, deformation modes and torsional vibrations around CC, SiC and SiSi bonds.

Methyl rocking vibrations. CH_3 rocking modes usually have significant intensities in the IR and Raman. In the present case, modes denoted by ρ_2CH_3 (a_u) and ρ_2CH_3 (b_g) display exceptional behaviour and elude observation. This is due to the fact that these symmetry coordinates belong to the symmetry species a_2 of a $C(CH_3)_3$ fragment assuming perfect C_{3v} symmetry (a_2 modes in C_{3v} are neither IR nor Raman active). The remaining methyl rocking vibrations are observed in the range from 1000 to 1200 cm^{-1} and are reasonably well characterised by a single symmetry coordinate.

CC and SiC stretches. CC stretches can be divided into $\nu_{sym}CC_3$ modes spanning the irreducible representations a_g and b_u and $\nu_{asym}CC_3$ modes transforming as $a_g + a_u + b_g + b_u$. Not surprisingly, the spectral positions of these modes are not affected by the nature of the substituents X on the central SiSi bond. $\nu_{sym}CC_3$ and $\nu_{asym}CC_3$ modes are observed at around 810 and 940 cm^{-1}, respectively.

SiC stretches transform as a_g and b_u, respectively. The calculated PED for these modes is comparable for the three *tert*-butyldisilanes under investigation in the present study. However, the calculated and observed frequencies increase in the order I ⟶ Br ⟶ Cl. This is readily attributed to an increase of the SiC stretching force constant with increasing electronegativity of the substituents X on the central SiSi bond.

SiX stretches. SiX stretching modes divide into $\nu_{sym}SiX_2$ ($a_g + b_u$) and $\nu_{asym}SiX_2$ ($a_u + b_g$) vibrations, respectively. As can be anticipated from a visualisation of vibrational motion, $\nu_{asym}SiX_2$ modes are less susceptible to vibrational mixing with other modes than $\nu_{sym}SiX_2$ modes and their PED is strongly dominated by a single symmetry coordinate. Similarly, the $\nu_{sym}SiX_2$ (b_u) mode is also reasonably well characterised by a

single symmetry coordinate, due to the absence of b_u modes suitable for kinetic coupling. In contrast, $\nu_{sym}SiX_2$ (a_g) modes are prone to strong vibrational mixing involving a multitude of a_g modes of similar vibrational energy. In $Bu^tCl_2SiSiCl_2Bu^t$, the symmetry coordinate $\nu_{sym}SiCl_2$ (a_g) is predicted to dominate the mode calculated at 581 cm^{-1}. However, this is the only mode containing strong admixtures from νSiSi (S_{11}) and hence has approximately been ascribed to the SiSi bond stretch. $\nu_{sym}SiCl_2$ (a_g) is then assigned to the mode predicted at 303 cm^{-1}. This assignment is also highly approximate since this mode is actually dominated by the symmetry coordinate ρCC_3 (S_8), which also dominates the mode calculated at 224 cm^{-1}. Even more curiously, calculations suggest that in Bu^tBr_2Si-$SiBr_2Bu^t$ $\nu_{sym}SiBr_2$ (a_g) is to be attributed to the mode calculated at 210 cm^{-1}, although this mode is dominated by a CC torsional mode (S_{25}), which in turn is the most important contributor in the mode computed at 221 cm^{-1}. The vibrational coupling involving stretching modes and torsional modes as predicted by the calculations might be questioned with respect to the fact that the calculations employ the harmonic approximation to model large amplitude torsional modes where it clearly is incorrect.

SiSi stretches. The SiSi stretching mode is calculated at 581, 528 and 501 cm^{-1} for X = Cl, Br and I, respectively. This agrees nicely with the trend one would predict from an increase of the SiSi stretching force constant with increasing electronegativity of the substituent X.

Deformation modes. Deformation modes are divided into two $\delta_{sym}CC_3$ modes (transforming as $a_g + b_u$), four $\delta_{asym}CC_3$ modes (transforming as $a_g + a_u + b_g + b_u$), four ρCC_3 modes (transforming as $a_g + a_u + a_g + b_u$), two δSiX_2 modes ($a_g + b_u$), two γSiX_2 modes ($a_g + b_u$), two ρSiX_2 modes ($a_u + b_g$), two τSiX_2 modes ($a_u + b_g$) and two δSiSiC modes ($a_g + b_u$). The deformation modes of the CC_3 fragments ($\delta_{sym}CC_3$, $\delta_{asym}CC_3$ and ρCC_3) are observed in the range from ≈200–450 cm^{-1}. It is of some note that the calculations predict heavy mixing between the symmetry coordinates ρCC_3 and τCC. Torsional vibrations around CC bonds thus gain intensity and τCC coordinates sometimes even dominate several vibrational modes. For example, in $Bu^tCl_2SiSiCl_2Bu^t$, the symmetry coordinate S_{39} [τ_2CC (b_g)] is the most important contribution in the modes calculated at 260 and 296 cm^{-1} and S_{54} (τCC) dominates the modes computed at 270 and 289 cm^{-1} (see Table S8, ESI). Vibrational coupling involving τCC_3 and τCC modes has also been predicted for the disilane Bu^tH_2SiSiH-Bu^t_2.[9] Again, this unexpected result might be due to artefacts in the calculations treating torsional vibrations as small amplitude vibrational motions.

The remaining deformation modes are observed below 200 cm^{-1} and the respective symmetry coordinates are strongly mixed with each other. These modes are not discussed further. Details of the calculated potential energy distributions are presented in Tables S8–10 (ESI).

Torsional vibrations. The molecules $Bu^tX_2SiSiX_2Bu^t$ possess six torsional vibrations around CC bonds, two torsional vibrations around SiC bonds and a single SiSi torsional mode. τSiC and τSiSi modes are found to be largely decoupled from deformation modes and stretching modes and reflect reasonable potential energy distributions and thus eluded observation. In contrast, as mentioned above, several τCC modes gain intensity by vibrational coupling and have tentatively been assigned to observed wavenumbers guided by the calculations.

Rotational isomerism

Variable temperature Raman spectroscopy is a useful tool for the investigation of conformational mixtures because Raman-active skeletal modes usually vary significantly with the backbone conformation. Previously the rotational isomers of the disilanes MeX_2SiSiX_2Me[35] and the trisilanes $SiMe_3SiMe_2$-$SiMe_2X$[36] and $SiMe_3SiMe_2SiMeX_2$[37] have been detected by this technique. For example, in $MeBr_2SiSiBr_2Me$ the wavenumber of the strongly Raman-active symmetric SiBr stetching mode ($\nu_{sym}SiBr_2$) was found to differ by 20 cm^{-1} between *anti* and *gauche* conformers. Unexpectedly, the calculated vibrational frequencies of transoid and twisted (*gauche* and *ortho*) conformers of the disilanes $Bu^tX_2SiSiX_2Bu^t$ (X = Cl, Br and I) are predicted to differ very little from each other and there is little hope of identifying rotational isomers from vibrational spectra of the condensed phases. Indeed, Raman spectra of liquid $Bu^tCl_2SiSiCl_2Bu^t$, liquid $Bu^tBr_2SiSiBr_2Bu^t$ and of a solution of $Bu^tI_2SiSiI_2Bu^t$ in various organic solvents are not sensitive to temperature and thus do not reveal clues about the existence of rotational isomers. Moreover, the vibrational spectra of solid $Bu^tBr_2SiSiBr_2Bu^t$ and $Bu^tI_2SiSiI_2Bu^t$ strictly follow the rule of mutual exclusion and this strongly suggests that the planar *anti* rotamer (point group C_{2h}) is the only structure present in the solid state. However, this is not true for $Bu^tCl_2SiSiCl_2Bu^t$. For the transoid conformer, the modes $\delta_{sym}CC_3$ (a,a_g) and νSiSi (a,a_g) are predicted to have fairly high intensities in the Raman whereas the intensities in the IR are very small. In the solid state these modes are tentatively assigned to the peaks at around 437 and 585 cm^{-1}. Surprisingly, the IR spectrum of solid Bu^tCl_2Si-$SiCl_2Bu^t$ also shows two rather strong peaks at similar positions (443 and 587 cm^{-1}). This suggests that a substantial fraction of twisted conformers (*gauche* and/or *ortho*) is present in solid $Bu^tCl_2SiSiCl_2Bu^t$ as only the twisted structures are predicted to possess high IR intensities at these spectral positions. The calculated amount of twisted conformers present is ≈10%. This agrees with that predicted in the gas-phase by *ab initio* calculations with 94% transoid and ≈3% each of the other two conformers. As the solid was formed by sublimation, the presence of these bands can thus be explained, although no other conformers were observed in the crystal structure of the solid.

Discussion

Theoretical and experimental studies show that 1,2-di-*tert*-butyltetrachlorodisilane exists as a single conformer in the gas phase, with a φ(C–Si–Si–C) dihedral angle of 168°.

The final experimental structure is in satisfactory agreement with that calculated *ab initio* at the MP2/6-31G* level; computed bond lengths and angles generally fall within 1–2 pm or 1–2° of the GED values (Table 4). For example, the Si–Si bond length refined to 238.0(7) pm compared to the computed value of 235.8 pm. The mean C–C bond length refined to 154.3(2) pm compared to 153.6 pm (mean) from the calculations and the Si–C bond length was 187.2(7) pm compared to the calculated value of 188.9 pm. The experimental Si–Cl (mean) bond length (207.1 pm) compared very well with the calculated value of 207.2 pm. The Si–Si–C bond angle refined to 119.8(6)° compared with the predicted value of 117.6° and the Cl–Si–Cl bond angle refined to 105.5(8)° compared to the calculated value of 107.4°. The torsion about the Si–Si axis, dihedral angle C(11)–Si(1)–Si(2)–C(21), which uniquely describes the position of the butyl groups about the Si–Si axis, agrees extremely well with the predicted value; 167.7(11) *vs.* 167.9°.

Observed geometric parameters are generally consistent with those for a number of closely related compounds. For example, the Si–Si bond distance in 1,2-di-*tert*-butyltetrachlorodisilane [238.0(7) pm] is within the range of values found for other disilanes from GED refinements, including 1,2-diiododisilane[6] [238.0(34) pm] and 1,1,2,2-tetraiododisilane[6] [238.9(37) pm] and 1,1,2-tri-*tert*-butyldisilane[9] [236.3(8) pm]. It is somewhat longer than those in some other halogenated and/or bulky disilanes, including 1,2-di-*tert*-butyldisilane[7] [234.8(3) pm] and

1,1,2,2-tetrabromodisilane[5] [234.9(19) pm]. However, 1,1,2,2-tetrachlorodisilane[32] is reported as having a Si–Si bond length of only 231.0(8) pm. This gives an indication that the bulky alkyl ligands have a large steric effect on the bond lengths within the molecule, as might be expected. Refined values of the C–C [154.3(2) pm] and Si–Cl [207.1(1) pm] bond lengths are in excellent agreement with calculated values, but again, the Si–Cl bonds were found to be much longer in 1,2-di-*tert*-butyltetrachlorodisilane than in 1,1,2,2-tetrachlorodisilane[32] [203.9(2) pm]. This may be a steric effect of the bulky alkyl groups at each end of the molecule, but may also be influenced by the electron-releasing properties of these groups. Both types of effect must play significant roles in determining bond distances in disilanes.

The dramatic deviation of the Si–Si–C bond angle [119.8(6)°] from the "pure" sp^3 tetrahedral angle (109.5°) is a common feature of disilanes with butyl groups. For example, in 1,1,2-tri-*tert*-butyldisilane[9] Si–Si–C angles of up to 116.0(8)° are observed, whilst 1,2-di-*tert*-butyldisilane[7] [113.7(3)°] and 1,2-di-*tert*-butyltetrafluorodisilane[8] [114.6(7)°] also demonstrate widening of the Si–Si–C angle. This provides more evidence for significant steric interaction between the butyl groups at one end of the molecule and chlorine atoms at the other end in 1,2-di-*tert*-butyltetrachlorodisilane.

The structure of 1,1,2,2-tetrachlorodisilane has recently been reported.[32] Johansen and co-workers report that in the gas phase there is a mixture of two conformers, *anti* [φ(HSiSiH) = 180°] and *gauche* [φ(HSiSiH) ≈ 60°]. In this case, however, the *gauche* conformer was found to predominate in the gas phase mixture, existing in an 80 : 20% ratio with the *anti* conformer. This is in complete contrast to the di-*tert*-butyl substituted case, where the *anti* conformation was found to be dominant in the gas phase. This is yet more evidence for steric crowding amongst these bulky alkyl substituted disilanes.

The solid-state structure of 1,2-di-*tert*-butyltetrachlorodisilane was also determined. The space group $P\bar{1}$ indicates that the molecule has an inversion centre, and thus the C–Si–Si–C dihedral angle is 180.0° as opposed to the C_2 structure [φ(CSiSiC) = 167.7(11)°] found in the gas phase. Thermal parameters associated with the solid structure were investigated to ascertain whether there was much disorder within the crystal, given the change in the C–Si–Si–C torsion angle between the solid and gaseous structures indicating that there are intermolecular forces acting on the solid. There was found to be a slight distortion of the carbon and chlorine atoms in the *y* direction, but no significant distortion was detected.

Bond lengths and angles agree in the solid and gaseous structures very well. For example, the Si–C bond length was found to be 188.1(3) pm in the solid compared to 187.2(7) in the gas. The mean C–C distances also agree extremely well [solid 154.3(4) pm; gas 154.3(2) pm] as do the mean Si–Cl distances [solid 206.3(1) pm; gas 207.1(1) pm]. There is a slight discrepancy between the experimental Si–Si distances, 236.9(1) pm in the solid, 238.0(7) pm in the gas. However, this is not a major difference when one considers the uncertainties associated with both distances.

Angles were also found to agree well between the solid and gaseous phases, with the Si–Si–C angle found to be 118.2(9)° in the solid phase compared to 119.8(6)° in the gas phase. The Cl–Si–Cl angle refined to 106.9(5)° in the crystal compared to 105.5(8)° in the GED refinement. The mean C–C–C angles, 109.4(2) and 109.1(3)° in the solid and gas phases, also agree well.

The crystal structures of the bromo and iodo analogues were also determined. Unfortunately, they are not volatile enough to collect GED data, but we can compare the crystal structures with each other, and with those calculated *ab initio*. Both structures were found to behave very similarly to the chloro analogue in the solid phase, *i.e.* possessing $P\bar{1}$ symmetry with an inversion centre at the centre of the Si–Si bond. Si–Si bond lengths in 1,2-di-*tert*-butyltetrabromodisilane and 1,2-di-*tert*-butyltetraiododisilane were found to be very similar to each other and to that found in 1,2-di-*tert*-butyltetrachlorodisilane; 235.4 pm in 1,2-di-*tert*-butyltetrabromodisilane and 236.6 pm in 1,2-di-*tert*-butyltetraiododisilane compared to 236.9 pm in 1,2-di-*tert*-butyltetrachlorodisilane. A slight variation in the Si–C bond lengths was found, with 189.7 pm in 1,2-di-*tert*-butyltetrabromodisilane and 190.4 pm in 1,2-di-*tert*-butyltetraiododisilane compared to 188.1 pm in 1,2-di-*tert*-butyltetrachlorodisilane. The mean C–C bond lengths were all consistent with each other; 153.8 pm in 1,2-di-*tert*-butyltetrabromodisilane and 154.0 pm in 1,2-di-*tert*-butyltetraiododisilane compared to 154.3 pm in 1,2-di-*tert*-butyltetrachlorodisilane.

The C–C–C angles were also found to be very consistent (1,2-di-*tert*-butyltetrachlorodisilane 109.4, 1,2-di-*tert*-butyltetrabromodisilane 110.1 and 1,2-di-*tert*-butyltetraiododisilane 109.2°), indicating very little steric strain within the butyl groups themselves. The S–Si–C angles were found to increase from X = Cl to I (Cl 118.2; Br 119.2; I 120.0°), as did the X–Si–X angles (Cl 106.9; Br 107.6; I 108.1°). This is to be expected on steric and electronic grounds. Electronically, chlorine is more electron-withdrawing than bromine and iodine, thus Cl–Si–Cl is smaller than Br–Si–Br and I–Si–I. Sterically, as the halogen increases in size, the X–Si–X angle would be expected to increase, as would the Si–Si–C angle at the opposing end of the molecule. However, this increase is offset by steric constraints of the halogens at the same end of the molecule.

Acknowledgements

We thank the EPSRC for financial support of the Edinburgh Electron Diffraction Service (grant GR/K44411) and for the Edinburgh *ab initio* facilities (grant GR/K04194). We also thank Dr V. Typke of the University of Ulm for the variable-array version of ASYM40, the Austrian 'Fonds zur Förderung der wissenschaftlichen Forschung' for financial support (projects P-10283-CHE and S-07904-CHE) and the UK Computational Facility (admin: Department of Chemistry, King's College London, Strand, London, UK WC2R 2LS) for computing time on Columbus.

References

1 B. Beagley, A. R. Conrad, J. M. Freeman, J. J. Monaghan, B. G. Norton and G. C. Holywell, *J. Mol. Struct.*, 1972, **11**, 371.
2 D. W. H. Rankin and A. Robertson, *J. Mol. Struct.*, 1975, **27**, 438.
3 Y. Morino and E. Hirota, *J. Chem. Phys.*, 1958, **28**, 185.
4 B. Beagley, J. J. Monaghan and T. G. Hewitt, *J. Mol. Struct.*, 1971, **8**, 401.
5 H. Thomassen, K. Hagen, R. Stølevik and K. Hassler, *J. Mol. Struct.*, 1986, **147**, 331.
6 E. Røhmen, K. Hagen, R. Stølevik, K. Hassler and M. Pöschl, *J. Mol. Struct.*, 1991, **244**, 41.
7 D. Hnyk, R. S. Fender, H. E. Robertson, D. W. H. Rankin, M. Bühl, K. Hassler and K. Schenzel, *J. Mol. Struct.*, 1995, **346**, 215.
8 B. A. Smart, H. E. Robertson, N. W. Mitzel, D. W. H. Rankin, R. Zink and K. Hassler, *J. Chem. Soc., Dalton Trans.*, 1997, 2475.
9 S. L. Hinchley, B. A. Smart, C. A. Morrison, H. E. Robertson, D. W. H. Rankin, R. Zink and K. Hassler, *J. Chem. Soc., Dalton Trans.*, 1999, 2303.
10 B. Reiter and K. J. Hassler, *J. Organomet. Chem.*, 1994, **467**, 21.
11 Gaussian 94 (Revision C.2), M. J. Frisch, G. W. Trucks, H. B. Schlegel, P. M. W. Gill, B. G. Johnson, M. A. Robb, J. R. Cheeseman, T. A. Keith, G. A. Petersson, J. A. Montgomery, K. Raghavachari, M. A. Al-Laham, V. G. Zakrzewski, J. V. Ortiz, J. B. Foresman, J. Cioslowski, B. B. Stefanov, A. Nanayakkara, M. Challacombe, C. Y. Peng, P. Y. Ayala, W. Chen, M. W. Wong, J. L. Andres, E. S. Replogle, R. Gomperts, R. L. Martin, D. J. Fox, J. S. Binkley, D. J. Defrees, J. Baker, J. P. Stewart, M. Head-Gordon, C. Gonzalez and J. A. Pople, Gaussian Inc., Pittsburgh, PA, 1995.
12 Gaussian 98 (Revision A.7), M. J. Frisch, G. W. Trucks, H. B. Schlegel, G. E. Scuseria, M. A. Robb, J. R. Cheeseman, V. G. Zakrzewski, J. A. Montgomery, R. E. Stratmann, Jr., J. C. Burant, S. Dapprich, J. M. Millam, A. D. Daniels, K. N. Kudin,

M. C. Strain, O. Farkas, J. Tomasi, V. Barone, M. Cossi, R. Cammi, B. Mennucci, C. Pomelli, C. Adamo, S. Clifford, J. Ochterski, G. A. Petersson, P. Y. Ayala, Q. Cui, K. Morokuma, D. K. Malick, A. D. Rabuck, K. Raghavachari, J. B. Foresman, J. Cioslowski, J. V. Ortiz, A. G. Baboul, B. B. Stefanov, G. Liu, A. Liashenko, P. Piskorz, I. Komaromi, R. Gomperts, R. L. Martin, D. J. Fox, T. Keith, M. A. Al-Laham, C. Y. Peng, A. Nanayakkara, C. Gonzalez, M. Challacombe, P. M. W. Gill, B. Johnson, W. Chen, M. W. Wong, J. L. Andres, C. Gonzalez, M. Head-Gordon, E. S. Replogle and J. A. Pople, Gaussian, Inc., Pittsburgh, PA, 1998.
13 J. S. Binkley, J. A. Pople and W. J. Hehre, *J. Am. Chem. Soc.*, 1980, **102**, 939.
14 M. S. Gordon, J. S. Binkley, J. A. Pople, W. J. Pietro and W. J. Hehre, *J. Am. Chem. Soc.*, 1982, **104**, 2797.
15 W. J. Pietro, M. M. Francl, W. J. Hehre, D. J. DeFrees, J. A. Pople and J. S. Binkley, *J. Am. Chem. Soc.*, 1982, **104**, 5039.
16 W. J. Hehre, R. Ditchfield and J. A. Pople, *J. Chem. Phys.*, 1972, **56**, 2257.
17 P. C. Hariharan and J. A. Pople, *Theor. Chim. Acta*, 1973, **28**, 213.
18 M. S. Gordon, *Chem. Phys. Lett.*, 1980, **76**, 163.
19 W. Stevens, H. Basch and J. Krauss, *J. Chem. Phys.*, 1984, **81**, 6026.
20 W. Stevens, J. Krauss, H. Basch and P. G Jasien, *Can. J. Chem.*, 1992, **70**, 612.
21 T. R. Cundari and W. J. Stevens, *J. Chem. Phys.*, 1993, **98**, 5555.
22 H. A. Fogarty, C. H. Ottoson and J. Michl, *J. Mol. Struct.*, 2000, **556**, 105.
23 G. M. Sheldrick, SHELXTL, version 5.1, Bruker AXS, Madison, WI, USA, 1998.
24 C. M. Huntley, G. S. Laurenson and D. W. H. Rankin, *J. Chem. Soc., Dalton Trans.*, 1980, 954.
25 J. R. Lewis, P. T. Brain and D. W. H. Rankin, *Spectrum*, 1997, **15**, 7.
26 S. Cradock, J. Koprowski and D. W. H. Rankin, *J. Mol. Struct.*, 1981, **77**, 113.
27 A. S. F. Boyd, G. S. Laurenson and D. W. H. Rankin, *J. Mol. Struct.*, 1981, **71**, 217.
28 A. W. Ross, M. Fink and R. Hilderbrandt, in *International Tables for Crystallography*, A. J. C. Wilson, ed., vol. C, Kluwer Academic Publishers, Dordrecht, 1992, p. 245.
29 A. J. Blake, P. T. Brain, H. McNab, J. Miller, C. A. Morrison, S. Parsons, D. W. H. Rankin, H. E. Robertson and B. A. Smart, *J. Phys. Chem.*, 1996, **100**, 12280; P. T. Brain, C. A. Morrison, S. Parsons and D. W. H. Rankin, *J. Chem. Soc., Dalton Trans.*, 1996, 4589.
30 N. W. Mitzel, B. A. Smart, A. J. Blake, H. E. Robertson and D. W. H. Rankin, *J. Phys. Chem.*, 1996, **100**, 9339.
31 K. Kveseth, *Acta Chem. Scand., Ser. A*, 1979, **33**, 453.
32 T. H. Johansen, K. Hagen and R. Stølevik, *J. Mol. Struct.*, 1999, **485–486**, 121.
33 L. Hedberg and I. M. Mills, *J. Mol. Spectrosc.*, 1993, **160**, 117.
34 E. B. Wilson, Jr., J. C. Decius and P. C. Cross, *Molecular Vibrations*, McGraw-Hill, New York, 1955.
35 R. Zink, K. Hassler and M. Ramek, *Vib. Spectrosc.*, 1998, **18**, 123.
36 A. Jähn, K. Schenzel, R. Zink and K. Hassler, *J. Raman Spectrosc.*, 1998, **29**, 841.
37 A. Jähn, K. Schenzel, R. Zink and K. Hassler, *J. Raman Spectrosc.*, 1998, **29**, 1055.